Frontiers of Physics
https://doi.org/10.1007/s11467-019-0897-0
Front. Phys.
14(5), 53602 (2019)

RESEARCH ARTICLE

Skyrmion Hall effect with spatially modulated Dzyaloshinskii–Moriya interaction

Liping Zhou*, Ren Qin*, Ya-Qing Zheng, Yong Wang†

School of Physics, Nankai University, Tianjin 300071, China
Corresponding author. E-mail: †yongwang@nankai.edu.cn
Received February 28, 2019; accepted March 20, 2019

The skyrmion Hall effect is theoretically studied in the chiral ferromagnetic film with spatially modulated Dzyaloshinskii–Moriya interaction. Three cases including linear, sinusoidal, and periodic rectangular modulations have been considered, where the increase, decrease, and the periodic modification of the size and velocity of the skyrmion have been observed in the microscopic simulations. These phenomena are well explained by the Thiele equation, where an effective force on the skyrmion is induced by the inhomogeneous Dzyaloshinskii–Moriya interaction. The results here suggest that the skyrmion Hall effect can be manipulated by artificially tuning the Dzyaloshinskii–Moriya interaction in chiral ferromagnetic film with material engineering methods, which will be useful to design skyrmion-based spintronics devices.

Keywords magnetic skyrmion, skyrmion Hall effect, Thiele equation

1 Introduction

In recent years, the discovery of magnetic skyrmion in chiral ferromagnetic materials has triggered extensive research activities [1–18, 20–22], mainly due to its potential applications in spintronics devices [23–27]. The broken inversion symmetry of the materials will induce finite Dzyaloshinskii–Moriya interaction (DMI) [28, 29], which can stabilize the magnetic skyrmion together with the Heisenberg exchange interaction, external magnetic field or the magnetocrystalline anisotropy field. The dynamics of the skyrmion can be flexibly manipulated by spin-polarized current [14, 15], and the trajectory of its center can be simply described by the Thiele equation [23]. It shows that a transverse component of the velocity will be generated by an effective force on the skyrmion, i.e., "the skyrmion Hall effect" [15], which has been confirmed in recent experimental observations [20, 21].

Meanwhile, the physical factors influencing the DMI in chiral ferromagnetic materials have been carefully investigated [30–40]. For instance, it has been shown that the bulk DMI can be modified by the chemical composition [30], carrier density and the strain [31], band filling [35], etc. The interfacial DMI in the multilayer thin films, on the other hand, can be tuned by the thickness of certain layer [32, 39, 40], oxygen coverage [33], ion irradiation [34], etc. Furthermore, the effect of electric field has also been studied [36, 37, 40], where 130% variation of DMI in Ta/FeCoB/TaO_x trilayer has been demonstrated experimentally [36]. These developments thereby lay the foundation to control the dynamics of magnetic skyrmion by artificially modulating the DMI in chiral ferromagnetic materials [41, 42].

In this paper, we investigate the skyrmion Hall effect in a chiral ferromagnetic film with spatially modulated DMI. We show that the trajectory of the skyrmion will be drastically modified by the inhomogeneous DMI, which can be well understood by analyzing the Thiele equation. The results here will be beneficial to design skyrmion-based devices by controlling the DMI with material engineering techniques.

2 Theoretical model

As shown in Fig. 1, the model system is a chiral ferromagnetic film with length L, width w, and thickness d. The main interactions among the magnetic moments here include the Heisenberg exchange interaction, DMI, and the perpendicular magnetic anisotropy, which thus give the energy density of the film as [14, 15, 23]

$$\mathcal{E}[\boldsymbol{m}] = A(\nabla \boldsymbol{m})^2 + \mathcal{E}_{DM}[\boldsymbol{m}] - K_u(\boldsymbol{e}_z \cdot \boldsymbol{m})^2. \quad (1)$$

Here, $\boldsymbol{m}(\boldsymbol{r}) = \boldsymbol{M}(\boldsymbol{r})/M_s$ is the normalized magnetization distribution, and M_s is the saturation magnetization; A is the exchange stiffness; K_u is the perpendicular magnetic anisotropy coefficient, and $\boldsymbol{e}_z$ is the anisotropic axis along z-direction. $\mathcal{E}_{DM}[\boldsymbol{m}]$ represents the energy density due to DMI interaction, where $\mathcal{E}_{DM}[\boldsymbol{m}] = D(m_z\nabla\cdot\boldsymbol{m} - \boldsymbol{m}\cdot\nabla m_z)$ for interfacial DMI and $\mathcal{E}_{DM}[\boldsymbol{m}] = D\boldsymbol{m}\cdot\nabla\times\boldsymbol{m}$ for bulk DMI [14, 15, 23, 43]. The coefficient D determines the strength of DMI and is assumed to be spatially inhomo-

*These two authors contributed equally to the work.
arXiv: 1901.02120.

© Higher Education Press and Springer-Verlag GmbH Germany, part of Springer Nature 2019

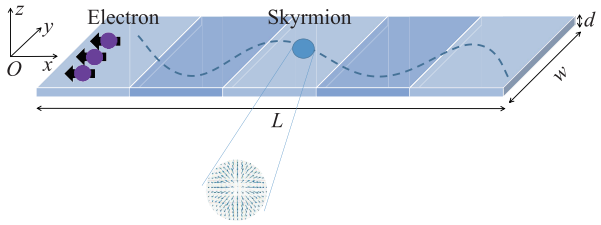

Fig. 1 Schematic diagram of the system under consideration. A chiral ferromagnetic film with spatially modulated Dzyaloshinskii–Moriya interaction is placed in the x-y plane. Spin-polarized electrons are injected to drive the motion of the magnetic skyrmion in the film. L: Length; w: Width; d: Thickness.

geneous.

A magnetic skyrmion will be prepared near the upper-left corner of the film, and a spin-polarized current perpendicular to the film will be applied. The amplitude, degree and direction of spin polarization of the applied current are denoted by I, p, $\boldsymbol{m}_p$, respectively. Then the magnetization dynamics of the film will be described by the Landau–Lifshitz–Gilbert–Slonczewski (LLGS) equation

$$\frac{\mathrm{d}\boldsymbol{m}}{\mathrm{d}t} = -\gamma_0 \boldsymbol{m} \times \boldsymbol{H}_{eff} + \alpha \boldsymbol{m} \times \frac{\mathrm{d}\boldsymbol{m}}{\mathrm{d}t} - \beta \boldsymbol{m} \times (\boldsymbol{m} \times \boldsymbol{m}_p). \tag{2}$$

Here, γ_0 is the gyromagnetic ratio; $\boldsymbol{H}_{eff} = -\frac{1}{M_s}\nabla_{\boldsymbol{m}}\mathcal{E}[\boldsymbol{m}]$ is the effective magnetic field; α is the Gilbert damping coefficient. The last term in Eq. (2) is the Slonczewski spin transfer torque with the amplitude $\beta = \frac{\gamma_0 \hbar I p}{2dM_s e}$, where $\hbar$ and e are the reduced Planck constant and elementary charge, respectively. The solution of Eq. (2) will give the current-driven dynamics of the skyrmion.

If the spatial variation of the DMI is small enough in the scale of the skyrmion size, we can approximately describe the structure of the skyrmion with fixed DMI strength D at its center. Its trajectory then can be described by the Thiele equation (see Appendix A) [44]

$$\hat{\mathcal{G}}\boldsymbol{v} - \alpha\hat{\mathcal{D}}\boldsymbol{v} - \boldsymbol{F} - \boldsymbol{F}^s = 0. \tag{3}$$

Here, $\boldsymbol{v}$ is the drift velocity of the skyrmion center; $\hat{\mathcal{G}}$ and $\hat{\mathcal{D}}$ denote the gyromagnetic coupling tensor and dissipative force tensor; $\boldsymbol{F}$ and $\boldsymbol{F}^s$ are the effective forces acting on the skyrmion due to the inhomogeneous energy density and the spin transfer torque, respectively. They are explicitly related to the magnetization distribution $\boldsymbol{m}(\boldsymbol{r})$ as

$$\hat{\mathcal{G}}_{\xi'\xi} = \int \mathrm{d}\boldsymbol{r}(\partial_{\xi'}\boldsymbol{m} \times \partial_{\xi}\boldsymbol{m}) \cdot \boldsymbol{m}, \tag{4}$$

$$\hat{\mathcal{D}}_{\xi'\xi} = \int \mathrm{d}\boldsymbol{r}\partial_{\xi'}\boldsymbol{m} \cdot \partial_{\xi}\boldsymbol{m}, \tag{5}$$

$$F_{\xi} = -\frac{\gamma_0}{M_s d}\int \mathrm{d}\boldsymbol{r}\partial_{\xi}\mathcal{E}[\boldsymbol{m}(\boldsymbol{r})], \tag{6}$$

$$F^s_{\xi} = \beta \int \mathrm{d}\boldsymbol{r}(\partial_{\xi}\boldsymbol{m} \times \boldsymbol{m}) \cdot \boldsymbol{m}_p. \tag{7}$$

The variables ξ, ξ' here denote the spatial coordinates x, y. Then the velocity $\boldsymbol{v}$ of the skyrmion will be obtained from the Thiele equation as

$$v_x = \frac{\mathcal{G}(F_y + F^s_y) - \alpha\mathcal{D}(F_x + F^s_x)}{\mathcal{G}^2 + \alpha^2\mathcal{D}^2}, \tag{8}$$

$$v_y = -\frac{\mathcal{G}(F_x + F^s_x) + \alpha\mathcal{D}(F_y + F^s_y)}{\mathcal{G}^2 + \alpha^2\mathcal{D}^2}, \tag{9}$$

which then gives the Hall angle $\vartheta_H = \arctan(v_y/v_x)$.

The interfacial and bulk DMI will result in Néel-type and Bloch-type skyrmion, respectively. In the polar coordinates taking the skyrmion center as the origin, the magnetization configuration of the skyrmion can be expressed as [23] $\boldsymbol{m}(r,\varphi) = (\sin\Theta(r)\cos\Phi(\varphi), \sin\Theta(r)\sin\Phi(\varphi), \cos\Theta(r))$, where $\Phi = \varphi + \gamma$. Depending on $D > 0$ or $D < 0$, the helicity γ will be 0 or π for the Néel-type skyrmion, and will be $\pi/2$ or $-\pi/2$ for the Bloch-type skyrmion (see Appendix B). Further calculations (see Appendix C) give the gyromagnetic coupling tensor $\hat{\mathcal{G}} = \begin{pmatrix} 0 & -\mathcal{G} \\ \mathcal{G} & 0 \end{pmatrix}$ with $\mathcal{G} = 4\pi$, and the dissipative force tensor $\hat{\mathcal{D}} = \begin{pmatrix} \mathcal{D} & 0 \\ 0 & \mathcal{D} \end{pmatrix}$, where

$$\mathcal{D} = \pi\int_0^{\infty}[r(\Theta')^2 + \frac{1}{r}\sin^2\Theta]\mathrm{d}r. \tag{10}$$

The force $\boldsymbol{F}$ due to the inhomogeneous DMI strength D is expressed as $\boldsymbol{F} = -\frac{2\gamma_0}{M_s}g_f\mathcal{F}\nabla D$. For convenience, we have defined the integral (see Appendix C)

$$\mathcal{F} = -\pi\int_0^{\infty}(r\Theta' + \sin\Theta\cos\Theta)\mathrm{d}r, \tag{11}$$

and the coefficient $g_f = \cos\gamma$ for Néel-type skyrmion and $g_f = \sin\gamma$ for Bloch-type skyrmion. When $\boldsymbol{m}_p = (\sin\theta\cos\phi, \sin\theta\sin\phi, \cos\theta)$, the force acting on the Néel-type skyrmion by the spin transfer torque is $\boldsymbol{F}^s = \cos\gamma(\sin\theta\sin\phi, -\sin\theta\cos\phi)\beta\mathcal{F}$, while the force on the Bloch-type skyrmion will be $\boldsymbol{F}^s = -\sin\gamma(\sin\theta\cos\phi, \sin\theta\sin\phi)\beta\mathcal{F}$.

The parameters in the Thiele equation (3) can be further estimated if the radial profile of the skyrmion $\Theta(r)$ is known, which then can predict the velocity of the skyrmion based on Eqs. (8) and (9). Here, we take the ansatz $\Theta(r) = 2\arctan[\frac{\sinh(R/w)}{\sinh(r/w)}]$ proposed recently [45], with the skyrmion radius $R = \pi D\sqrt{\frac{A}{16AK_u^2 - \pi^2D^2K_u}}$ and the skyrmion wall width $w = \frac{\pi D}{4K_u}$ [45]. In Fig. 2, R, w, $\mathcal{D}$, $\mathcal{F}$ are shown as the functions of DMI strength D by fixing the material parameters $A = 15$ pJ/m and $K_u = 0.8$ MJ/m^3. All of them will monotonically increase when D varies from 3 to 4 mJ/m^2.

3 Micromagnetic simulations

In this section, we investigate the current-driven dynamics of the magnetic skyrmion in the film by simulating the

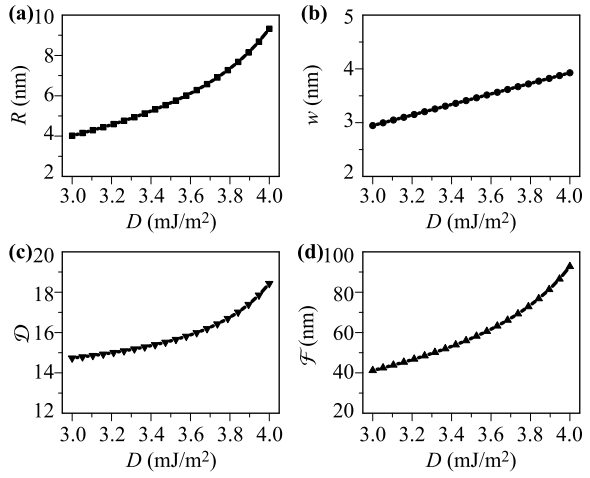

Fig. 2 **(a, b)** The dependence of the radius R and wall width w of the skyrmion on the DMI strength D according to the model in Ref. [45]. **(c, d)** The integrals $\mathcal{D}$ defined in Eq. (10) and $\mathcal{F}$ defined in Eq. (11) as functions of D. We have set $A = 15$ pJ/m and $K_u = 0.8$ MJ/m^3 in the calculations.

LLGS equation (2), and the simulated results are compared with the theoretical predictions from Thiele equation. The simulation parameters are set as $L = 500$ nm, $w = 100$ nm, $d = 0.4$ nm, $M_s = 5.8 \times 10^5$ A/m, $A = 15$ pJ/m, $K_u = 0.8$ MJ/m^3, $\alpha = 0.05$. The current amplitude is taken as $I = 3 \times 10^{11}$ A/m, with the degree of spin polarization $p = 0.4$. We restrict the simulations here to the case of Néel-type skyrmion, and set the direction of polarization $\boldsymbol{m}_p = (-1, 0, 0)$. The film is discretized into grids with size $1.0 \times 1.0 \times 0.4$ nm^3, and the time step during the simulations is taken as 1 fs for convergence.

3.1 Linear modulation

We first assume that the DMI strength is linearly modulated along the x-direction. In Fig. 3(a), the trajectories of the skyrmion are presented when D increases from 3 to 4 mJ/m^2 and decreases from 4 to 3 mJ/m^2, respectively. For comparison, the trajectory for homogeneous $D = 3.5$ mJ/m^2 is also shown. The results reveal that the Hall angle ϑ_H can be controlled by introducing the gradient of D. Besides, the size of the skyrmion will also vary when D is changed during the motion. In Figs. 2(b) and (c), the radius R and wall width w of the skyrmion are obtained by fitting the simulation results to the ansatz $\Theta(r) = 2\arctan[\frac{\sinh(R/w)}{\sinh(r/w)}]$. We see that the fitted R is generally larger than the theoretical value, which can be about 2 nm for large D. On the other hand, the fitted w is close to the theoretical values with a small difference about 0.3 nm. Therefore, we can take the proposed model in Ref. [45] to approximately estimate the profile of the skyrmion.

The velocity of the skyrmion is further determined from its trajectory, as shown in Figs. 3(d) and (e). As D is linearly increased from 3 to 4 mJ/m^2, both components of the velocity v_x and v_y will become larger. The force due to the linearly modulated D is along the x-direction and is given as $F_x = -\frac{2\gamma_0}{M_s}\mathcal{F}\nabla D$, while the force due to the spin transfer torque is along the y-direction with the value $F_y^s = \beta\mathcal{F}$. The Thiele equation will then give the velocity

$$v_x = \frac{\mathcal{G}\beta + \frac{2\gamma_0}{M_s}\alpha\nabla D\mathcal{D}}{\mathcal{G}^2 + \alpha^2\mathcal{D}^2}\mathcal{F}, \quad v_y = \frac{\frac{2\gamma_0}{M_s}\mathcal{G}\nabla D - \alpha\beta\mathcal{D}}{\mathcal{G}^2 + \alpha^2\mathcal{D}^2}\mathcal{F}.$$

Figure 2 has shown that $\mathcal{F}$ will quickly increase from 40 to 90 nm during the motion, thus both of v_x and v_y will increase along with the DMI strength D. Meanwhile, $\mathcal{D}$ will also slowly increase from 15 to 18 [see Fig. 2(c)], which thus explains the slight increase of the magnitude of Hall angle $\vartheta_H = \arctan(\frac{\frac{2\gamma_0}{M_s}\mathcal{G}\nabla D - \alpha\beta\mathcal{D}}{\mathcal{G}\beta + \frac{2\gamma_0}{M_s}\alpha\nabla D\mathcal{D}})$. Similarly, when D decreases from 4 to 3 mJ/m^2, the velocity v_x and v_y will both decrease, while the magnitude of the Hall angle ϑ_H will continuously decrease. Besides, the magnitude of Hall angle will be small for positive ∇D and be large for negative ∇D at fixed D, as shown in Figs. 3(a) and (f). Figures 3(d–f) suggest that the Thiele equation can correctly capture the trend of the velocity and Hall angle with linearly modulated D, although some quantitative differences exist.

3.2 Sinusoidal modulation

We further study the current-driven dynamics of skyrmion with a sinusoidal modulation of the DMI strength, where $D = 3.5 + 0.5\sin(2\pi x/100)$ mJ/m^2 with $x \in [0, 500]$ nm. Figure 4(a) shows that the trajectory of the skyrmion will be periodically distorted by the modulated DMI. Specially, the skyrmion will be pushed away but can always move back to the trajectory if D is set as 3.5 mJ/m^2. The behavior can be understood from the periodic modulation of the Hall angle, the magnitude of which will become large for negative ∇D and vice versa. The turning points x_0 of the trajectory will then be determined by the condition $\nabla D = 0$, which gives $x_0 = 25, 75, \cdots, 475$ nm. The skyrmion size will also be periodically modulated as expected. In Figs. 4(b) and (c), the radius R and wall width w of the skyrmion obtained by fitting the simulation results are compared to the theoretical values. The size of the skyrmion will expand and shrink periodically together with the DMI strength. In spite of quantitative differences, the theoretical calculations do can predict the variation of the skyrmion size satisfactorily.

The velocity $\boldsymbol{v}$ and Hall angle ϑ_H have also been obtained from the micromagnetic simulations and calculated from the Thiele equation separately. As shown in Figs. 4(d–f), $\boldsymbol{v}$ and ϑ_H will oscillate around the reference values obtained for fixed $D = 3.5$ mJ/m^2. Besides, v_x will achieve it maximal value when D is largest and vice versa, as determined by the factor $\mathcal{F}$ in Thiele equation. How-

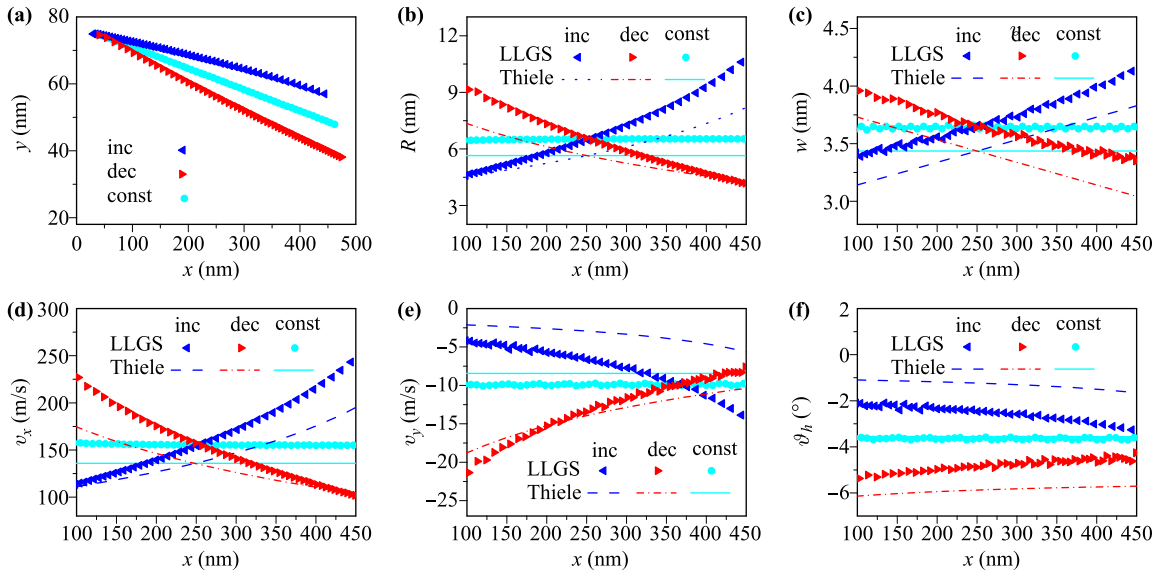

Fig. 3 **(a)** The trajectory of the skyrmion in the x–y plane of the film; **(b)** the location-dependent skyrmion radius R; **(c)** the location-dependent skyrmion wall width w; **(d, e)** the location-dependent velocity components v_x and v_y of the skyrmion; **(f)** the location-dependent Hall angle ϑ_H of the skyrmion. LLGS: Micromagnetic simulation based on LLGS equation (2); Thiele: Theoretical results based on Thiele equation. inc: D increases from 3 to 4 mJ/m^2 for $x \in [0, 500]$ nm; dec: D decreases from 4 to 3 mJ/m^2 for $x \in [0, 500]$ nm; const: D takes constant value 3.5 mJ/m^2 for comparison.

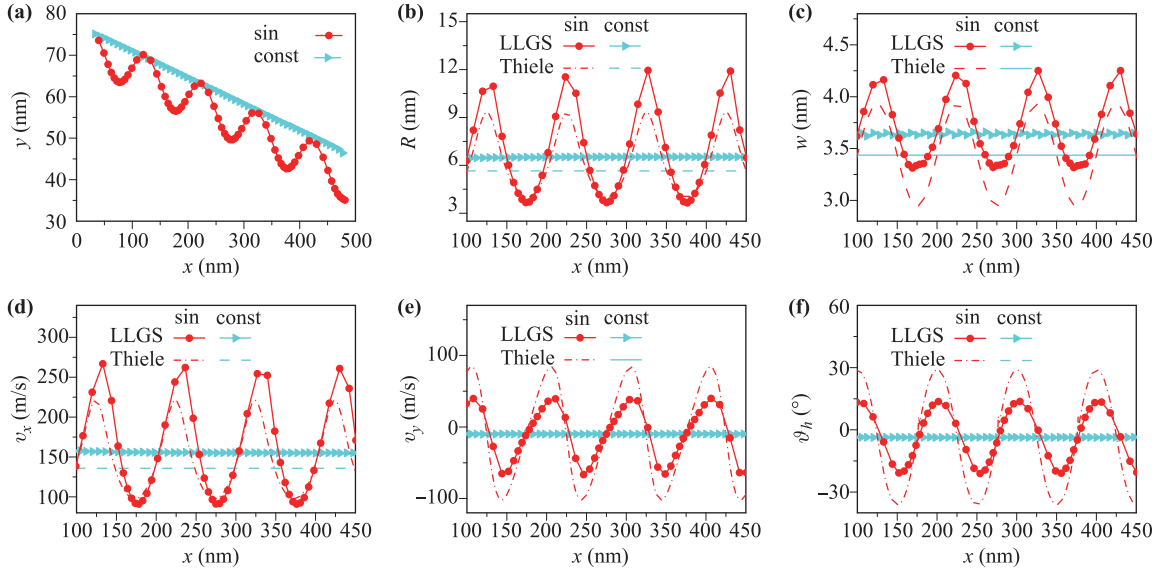

Fig. 4 **(a)** The trajectory of the skyrmion in the x–y plane of the film; **(b)** the location-dependent skyrmion radius R; **(c)** the location-dependent skyrmion wall width w; **(d, e)** the location-dependent velocity components v_x and v_y of the skyrmion; **(f)** the location-dependent Hall angle ϑ_H of the skyrmion. LLGS: Micromagnetic simulation based on LLGS equation (2); Thiele: Theoretical results based on Thiele equation. sin: D is sinusoidally modulated as $3.5 + 0.5\sin(2\pi x/100)$ mJ/m^2 for $x \in [0, 500]$ nm; const: D takes constant value 3.5 mJ/m^2 for comparison.

ever, v_y in this case can be either positive or negative, since ∇D here is large enough to be dominant. In the same reason, ϑ_H can also be positive or negative, which results in the "push-back" trajectory given in Fig. 4(a). Moreover, the Hall angle with maximally negative value will be achieved when ∇D is negatively largest at $x = 50$, 150, 250, 350, 450 nm, while the Hall angle with maximally positive value will be achieved at $x = 100$, 200, 300, 400 nm.

3.3 Periodic rectangular modulation

Finally, we consider the effect of the periodic rectangular modulation of DMI on the dynamics of skyrmion. In

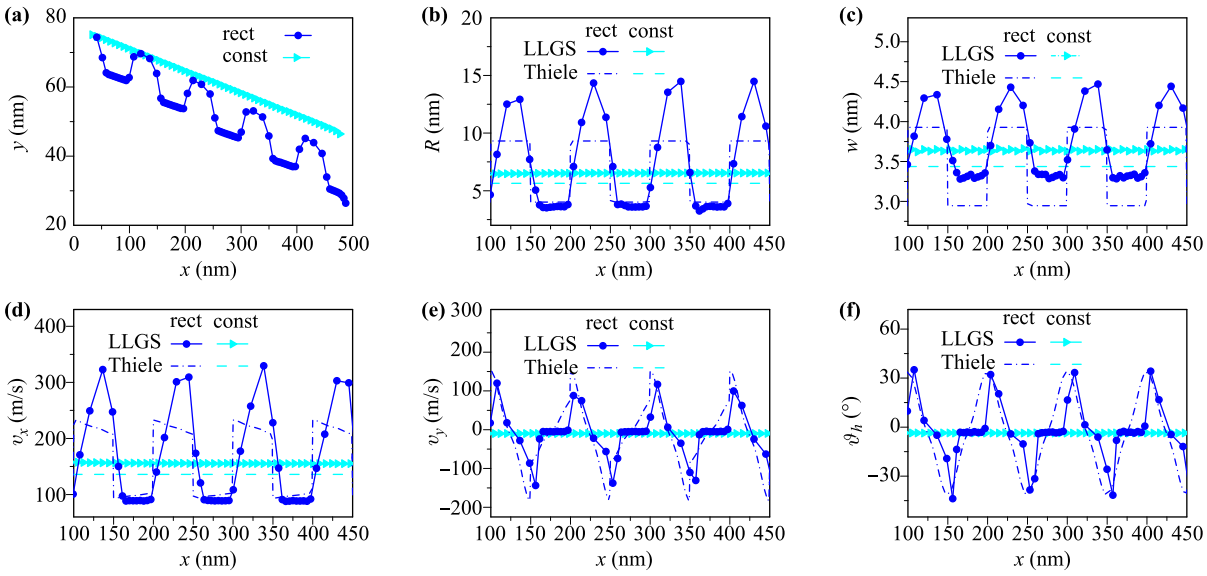

Fig. 5 **(a)** The trajectory of the skyrmion in the x–y plane of the film; **(b)** the location-dependent skyrmion radius R; **(c)** the location-dependent skyrmion wall width w; **(d, e)** the location-dependent velocity components v_x and v_y of the skyrmion; **(f)** the location-dependent Hall angle ϑ_H of the skyrmion. LLGS: Micromagnetic simulation based on LLGS equation (2); Thiele: Theoretical results based on Thiele equation. rect: D takes the values 4 mJ/m^2 or 3 mJ/m^2 alternately per 50 nm for $x \in [0, 500]$ nm; const: D takes constant value 3.5 mJ/m^2 for comparison.

Fig. 5(a), the trajectory of skyrmion has similar "push-back" feature, where D takes the values 4 mJ/m^2 or 3 mJ/m^2 alternately for each 50 nm along x-direction. Unlike the sinusoidal modulation case, the skyrmion size will be suddenly changed because of the abrupt increase or decrease of DMI; otherwise, the radius R and wall width w will be nearly the same in the regions with constant D [see Figs. 5(b, c)]. Once again, the agreement between the theoretical and simulated results will be better when D is small.

We have assumed that the modulation of DMI should be slow in the scale of the skyrmion size for the Thiele equation to be valid. This assumption will break down for the case here, since D is a step function of the location and ∇D will give the δ-pulsive force. Considering the finite size of the skyrmion, we exploit the Gaussian distribution $\frac{1}{\sqrt{\pi}\sigma}\mathrm{e}^{-\frac{x^2}{\sigma^2}}$ to replace the $\delta(x)$ function, where σ defines the broadening degree of the force $\boldsymbol{F}$. As shown in Figs. 5(d–f), the velocity $\boldsymbol{v}$ and Hall angle ϑ_H of the skyrmion are calculated from the Thiele equation by setting $\sigma = 15$ nm, which can reasonably explain the simulation results. Not surprisingly, $\boldsymbol{v}$ and ϑ_H will repeatedly modulated, and the direction of v_y will be changed to give the "push-back" motion in Fig. 5(a).

4 Discussion and conclusion

We notice that some quantitative differences exist between the results of micromagnetic simulation and the Thiele equation, which can be attributed to several reasons. Firstly, the analytical expressions for the skyrmion radius R and skyrmion wall width w exploited in the Thiele equation will only be accurate for the condition $R/w \gg 1$ [45], which however is not well satisfied for the magnetic skyrmion simulated here. Secondly, the structure of the skyrmion has been deformed by the inhomogeneous DMI, which further make the ansatz inaccurate to describe the magnetic skyrmion, especially if its size becomes large. Finally, numerical errors may be induced by the finite difference method during the micromagnetic simulations. Nevertheless, the Thiele equation can capture the correct physics to understand and predict the motion of the magnetic skyrmion discussed here.

In conclusion, we have investigated the skyrmion Hall effect in chiral ferromagnetic film with spatially modulated DMI based on the Thiele equation and the micromagnetic simulations. We show that the trajectory and size of skyrmion can be manipulated by tuning the Dzyaloshinskii–Moriya interaction. Specially, the motion of the skyrmion can be sped up or slowed down by the gradient of DMI, and periodic DMI will cause the "push-back" trajectory of the skyrmion. These phenomena could be realized by the material engineering technologies nowadays, e.g., applying a spatially modulated gate voltage. The results here will not only advance our understanding of the rich dynamics of magnetic skyrmion further, but also can be useful to develop novel skyrmion-based spintronics devices.

Acknowledgements This work was supported by the National Natural Science Foundation of China (Grant Nos. 61674083 and 11604162) and the Fundamental Research Funds for the Central Universities, Nankai University (No. 63191522).

Appendix A Derivation of Thiele equation

Here, we give the derivation of the Thiele equation from the LLGS equation (2). Taking the cross product of $\boldsymbol{m}$ and Eq. (2), we will get

$$\boldsymbol{m}\times\frac{\mathrm{d}\boldsymbol{m}}{\mathrm{d}t}=-\gamma_0\boldsymbol{m}\times(\boldsymbol{m}\times\boldsymbol{H}_{eff})+\alpha\boldsymbol{m}\times\left(\boldsymbol{m}\times\frac{\mathrm{d}\boldsymbol{m}}{\mathrm{d}t}\right)-\beta\boldsymbol{m}\times(\boldsymbol{m}\times(\boldsymbol{m}\times\boldsymbol{m}_p)),\tag{A1}$$

which can further reduce to

$$\boldsymbol{m}\times\frac{\mathrm{d}\boldsymbol{m}}{\mathrm{d}t}=-\gamma_0(\boldsymbol{m}\cdot\boldsymbol{H}_{eff})\boldsymbol{m}+\gamma_0\boldsymbol{H}_{eff}-\alpha\frac{\mathrm{d}\boldsymbol{m}}{\mathrm{d}t}+\beta\boldsymbol{m}\times\boldsymbol{m}_p.\tag{A2}$$

Here, we have applied the rule of vector triple product $\boldsymbol{a}\times(\boldsymbol{b}\times\boldsymbol{c})=\boldsymbol{b}(\boldsymbol{a}\cdot\boldsymbol{c})-\boldsymbol{c}(\boldsymbol{a}\cdot\boldsymbol{b})$ and the relations $\boldsymbol{m}\cdot\boldsymbol{m}=1,\boldsymbol{m}\cdot\frac{\mathrm{d}\boldsymbol{m}}{\mathrm{d}t}=0$. Assuming that the magnetization distribution of the skyrmion is not deformed during its motion, which is given as $\boldsymbol{m}(\boldsymbol{\xi})$ with the local coordinates $\boldsymbol{\xi}$ relative to its center $\boldsymbol{R}(t)$, then the magnetization distribution of the whole film in the lab coordinates will be $\boldsymbol{m}(\boldsymbol{r}-\boldsymbol{R}(t))=\boldsymbol{m}(\boldsymbol{\xi})$, and we will have $\frac{\mathrm{d}\boldsymbol{m}}{\mathrm{d}t}=-\boldsymbol{v}\cdot\nabla_{\boldsymbol{\xi}}\boldsymbol{m}$ with the skyrmion velocity $\boldsymbol{v}=\frac{\mathrm{d}\boldsymbol{R}}{\mathrm{d}t}$. Substituting $\frac{\mathrm{d}\boldsymbol{m}}{\mathrm{d}t}$ into Eq. (A2) and taking the dot product with $\nabla_{\boldsymbol{\xi}'}\boldsymbol{m}$, we further get

$$-\nabla_{\boldsymbol{\xi}'}\boldsymbol{m}\cdot(\boldsymbol{m}\times\boldsymbol{v}\cdot\nabla_{\boldsymbol{\xi}}\boldsymbol{m})=\gamma_0\nabla_{\boldsymbol{\xi}'}\boldsymbol{m}\cdot\boldsymbol{H}_{eff}+\alpha(\boldsymbol{v}\cdot\nabla_{\boldsymbol{\xi}}\boldsymbol{m})\cdot\nabla_{\boldsymbol{\xi}'}\boldsymbol{m}+\beta\nabla_{\boldsymbol{\xi}'}\boldsymbol{m}\cdot(\boldsymbol{m}\times\boldsymbol{m}_p).\tag{A3}$$

After integrating over the whole film, Eq. (A3) will reduce to the Thiele equation as

$$\mathcal{Q}\boldsymbol{v}-\alpha\mathcal{D}\boldsymbol{v}-\boldsymbol{F}-\boldsymbol{F}^s=0.\tag{A4}$$

Here, $\mathcal{Q}$ is the gyromagnetic coupling tensor and $\mathcal{D}$ is the dissipative force tensor; $\boldsymbol{F}$ and $\boldsymbol{F}^s$ are the forces on the skyrmion due to the inhomogeneous energy density $\mathcal{E}[\boldsymbol{m}]$ and spin transfer torque, respectively. They are defined as the functions of the magnetization configuration $\boldsymbol{m}(\boldsymbol{r})$ as

$$\mathcal{Q}=\int\mathrm{d}\boldsymbol{r}(\nabla_{\boldsymbol{\xi}'}\boldsymbol{m}\times\nabla_{\boldsymbol{\xi}}\boldsymbol{m})\cdot\boldsymbol{m},$$
$$\mathcal{D}=\int\mathrm{d}\boldsymbol{r}\nabla_{\boldsymbol{\xi}'}\boldsymbol{m}\cdot\nabla_{\boldsymbol{\xi}}\boldsymbol{m},$$
$$\boldsymbol{F}=-\frac{\gamma_0}{M_s}\int\mathrm{d}\boldsymbol{r}\nabla_{\boldsymbol{\xi}'}\mathcal{E}[\boldsymbol{m}],$$
$$\boldsymbol{F}^s=\beta\int\mathrm{d}\boldsymbol{r}(\nabla_{\boldsymbol{\xi}'}\boldsymbol{m}\times\boldsymbol{m})\cdot\boldsymbol{m}_p.$$

Appendix B Magnetic skyrmion configuration

In the polar coordinates, the magnetization configuration the skyrmion is expressed by $\boldsymbol{m}(\boldsymbol{r})=(\sin\Theta(r)\cos\Phi(\varphi),\sin\Theta(r)\sin\Phi(\varphi),\cos\Theta(r))$. The components of $\nabla_{\boldsymbol{\xi}}\boldsymbol{m}$ are calculated as

$$\frac{\partial m_x}{\partial x}=\Theta'\cos\Theta\cos\Phi\cos\varphi+\frac{1}{r}\sin\Theta\sin\Phi\sin\varphi,$$
$$\frac{\partial m_x}{\partial y}=\Theta'\cos\Theta\cos\Phi\sin\varphi-\frac{1}{r}\sin\Theta\sin\Phi\cos\varphi,$$
$$\frac{\partial m_y}{\partial x}=\Theta'\cos\Theta\sin\Phi\cos\varphi-\frac{1}{r}\sin\Theta\cos\Phi\sin\varphi,$$
$$\frac{\partial m_y}{\partial y}=\Theta'\cos\Theta\sin\Phi\sin\varphi+\frac{1}{r}\sin\Theta\cos\Phi\cos\varphi,$$
$$\frac{\partial m_z}{\partial x}=-\Theta'\sin\Theta\cos\varphi,$$
$$\frac{\partial m_z}{\partial y}=-\Theta'\sin\Theta\sin\varphi.$$

Here, we have utilized the relations

$$\frac{\partial r}{\partial x}=\cos\varphi,\frac{\partial r}{\partial y}=\sin\varphi,\frac{\partial\varphi}{\partial x}=-\frac{1}{r}\sin\varphi,\frac{\partial\varphi}{\partial y}=\frac{1}{r}\cos\varphi.$$

Then the energy density $\mathcal{E}[\boldsymbol{m}]$ with the interfacial DMI reads

$$\mathcal{E}[\boldsymbol{m}]=A\left[(\Theta')^2+\frac{1}{r^2}\sin^2\Theta\right]-K_u\cos^2\Theta+D\left(\Theta'+\frac{1}{r}\sin\Theta\cos\Theta\right)\cos(\Phi-\varphi).\tag{B1}$$

The stable magnetization configuration is determined by minimizing the total energy $E[\Theta,\Phi]=\int\mathrm{d}\boldsymbol{r}\mathcal{E}[\boldsymbol{m}]$ with the variational principle $\delta E=0$, which results in the following equations:

$$D\left(\Theta'+\frac{1}{r}\sin\Theta\cos\Theta\right)\sin(\Phi-\varphi)=0,$$
$$\Theta''+\frac{1}{r}\Theta'-\left(\frac{1}{2r^2}+\frac{K_u}{2A}\right)\sin2\Theta+\frac{D}{Ar}\sin^2\Theta\cos(\Phi-\varphi)=0.$$

Therefore, the helicity $\gamma=\Phi-\varphi$ should be 0 or π, namely, Néel-type skyrmion. Besides, considering that $\Theta|_{r=0}=\pi$ and $\Theta|_{r\to\infty}=0$, the energy due to DMI will be minimized if $\gamma=0$ for $D>0$ or $\gamma=\pi$ for $D<0$.

Similarly, the energy density $\mathcal{E}[\boldsymbol{m}]$ with bulk DMI is

$$\mathcal{E}[\boldsymbol{m}]=A\left[(\Theta')^2+\frac{1}{r^2}\sin^2\Theta\right]-K_u\cos^2\Theta+D\left(\Theta'+\frac{1}{r}\sin\Theta\cos\Theta\right)\sin(\Phi-\varphi).\tag{B2}$$

The variational equation $\delta\int\mathrm{d}\boldsymbol{r}\mathcal{E}[\boldsymbol{m}]=0$ then results in the following equations:

$$D\left(\Theta'+\frac{1}{r}\sin\Theta\cos\Theta\right)\cos(\Phi-\varphi)=0,$$
$$\Theta''+\frac{1}{r}\Theta'-\left(\frac{1}{2r^2}+\frac{K_u}{2A}\right)\sin2\Theta+\frac{D}{Ar}\sin^2\Theta\sin(\Phi-\varphi)=0.$$

In this case, the skyrmion will be Bloch-type with the helicity $\gamma=\pi/2$ for $D>0$ or $\gamma=-\pi/2$ for $D<0$.

Appendix C Expressions of $\mathcal{Q}, \mathcal{D}, \boldsymbol{F}, \boldsymbol{F}^s$

We now determine the expressions of $\mathcal{Q}, \mathcal{D}, \boldsymbol{F}, \boldsymbol{F}^s$ for a magnetic skyrmion in terms of the polar coordinates. First, it is easy to see that the diagonal matrix elements $\mathcal{Q}_{xx} = \mathcal{Q}_{yy} = 0$. While for its non-diagonal matrix element, straightforward calculations give $\frac{\partial \boldsymbol{m}}{\partial x} \times \frac{\partial \boldsymbol{m}}{\partial y} = \frac{1}{r}\Theta' \sin\Theta \boldsymbol{m}$, therefore we can get

$$\mathcal{Q}_{xy} = -\mathcal{Q}_{yx} = \int_0^{\infty} \mathrm{d}r \int_0^{2\pi} \mathrm{d}\varphi \Theta' \sin\Theta = -4\pi, \tag{C1}$$

which is the well-known skyrmion number with a -4π multiplier [23].

In order to calculate $\mathcal{D}$, we first have

$$\frac{\partial \boldsymbol{m}}{\partial x} \cdot \frac{\partial \boldsymbol{m}}{\partial x} = (\Theta')^2 \cos^2\varphi + \frac{1}{r^2}\sin^2\Theta \sin^2\varphi,$$
$$\frac{\partial \boldsymbol{m}}{\partial y} \cdot \frac{\partial \boldsymbol{m}}{\partial y} = (\Theta')^2 \sin^2\varphi + \frac{1}{r^2}\sin^2\Theta \cos^2\varphi,$$
$$\frac{\partial \boldsymbol{m}}{\partial x} \cdot \frac{\partial \boldsymbol{m}}{\partial y} = ((\Theta')^2 - \frac{1}{r^2}\sin^2\Theta)\sin\varphi\cos\varphi.$$

Therefore, the non-diagonal matrix elements $\mathcal{D}_{xy} = \mathcal{D}_{yx} = 0$ due to the integral over φ from 0 to 2π. The diagonal matrix elements of $\mathcal{D}$ will be

$$\mathcal{D}_{xx} = \mathcal{D}_{yy} = \pi \int_0^{\infty} [r(\Theta')^2 + \frac{1}{r}\sin^2\Theta]\mathrm{d}r. \tag{C2}$$

The force $\boldsymbol{F}$ can be calculated from the energy density $\mathcal{E}[\boldsymbol{m}]$ given in Appendix B. Since we have assumed that the skyrmion is not deformed, the only non-zero contribution to the force $\boldsymbol{F}$ will come from the inhomogeneous D, which is a function of the skyrmion center $\boldsymbol{R}$. Since $\nabla_{\boldsymbol{\xi}} = -\nabla_{\boldsymbol{R}}$, we will have

$$\boldsymbol{F} = g_f \frac{2\pi\gamma_0}{M_s} \nabla D \int_0^{\infty} [r\Theta' + \sin\Theta\cos\Theta]\mathrm{d}r.$$

Here, the factor $g_f = \cos\gamma$ for Néel-type skyrmion and $g_f = \sin\gamma$ for Bloch-type skyrmion.

Finally, we calculate the force $\boldsymbol{F}^s$ due to the spin transfer torque. We first have

$$\partial_x \boldsymbol{m} \times \boldsymbol{m} = \begin{pmatrix} \Theta'\sin\Phi\cos\varphi - \frac{1}{r}\sin\Theta\cos\Theta\cos\Phi\sin\varphi \\ -\Theta'\cos\Phi\cos\varphi - \frac{1}{r}\sin\Theta\cos\Theta\sin\Phi\sin\varphi \\ \frac{1}{r}\sin^2\Theta\sin\varphi \end{pmatrix},$$

$$\partial_y \boldsymbol{m} \times \boldsymbol{m} = \begin{pmatrix} \Theta'\sin\Phi\sin\varphi + \frac{1}{r}\sin\Theta\cos\Theta\cos\Phi\cos\varphi \\ -\Theta'\cos\Phi\sin\varphi + \frac{1}{r}\sin\Theta\cos\Theta\sin\Phi\cos\varphi \\ -\frac{1}{r}\sin^2\Theta\cos\varphi \end{pmatrix}.$$

For Néel-type skyrmion where $\Phi = \varphi$ or $\Phi = \varphi + \pi$, only the y-component of $\int \mathrm{d}\boldsymbol{r}(\partial_x \boldsymbol{m} \times \boldsymbol{m})$ and the x-component of $\int d\boldsymbol{r}(\partial_y \boldsymbol{m} \times \boldsymbol{m})$ are not zero after integral over φ. While for Bloch-type skyrmion where $\Phi = \varphi \pm \frac{\pi}{2}$, only the x-component of $\int \mathrm{d}\boldsymbol{r}(\partial_x \boldsymbol{m} \times \boldsymbol{m})$ and the y-component of $\int \mathrm{d}\boldsymbol{r}(\partial_y \boldsymbol{m} \times \boldsymbol{m})$ are not zero after the integral. Therefore, if $\boldsymbol{m}_p = (\sin\theta\cos\phi, \sin\theta\sin\phi, \cos\theta)$, the force acting on the Néel-type skyrmion will be

$$\boldsymbol{F}^s = \cos\gamma(\sin\theta\sin\phi, -\sin\theta\cos\phi)\beta\mathcal{F}, \tag{C3}$$

while the force acting on the Bloch-type skyrmion will be

$$\boldsymbol{F}^s = -\sin\gamma(\sin\theta\cos\phi, \sin\theta\sin\phi)\beta\mathcal{F}. \tag{C4}$$

Here, we have introduced the notation

$$\mathcal{F} = -\pi \int_0^{\infty} (r\Theta' + \sin\Theta\cos\Theta)\mathrm{d}r,$$

which has already appeared in the expression for $\boldsymbol{F}$.

References

1. A. N. Bogdanov and A. Hubert, Thermodynamically stable magnetic vortex states in magnetic crystals, *J. Magn. Magn. Mater.* 138(3), 255 (1994)
2. A. N. Bogdanov and A. Hubert, The stability of vortex-like structures in uniaxial ferromagnets, *J. Magn. Magn. Mater.* 195(1), 182 (1999)
3. A. N. Bogdanov and U. K. Rößler, Chiral symmetry breaking in magnetic thin films and multilayers, *Phys. Rev. Lett.* 87(3), 037203 (2001)
4. U. K. Rößler, A. N. Bogdanov, and C. Pfleiderer, Spontaneous skyrmion ground states in magnetic metals, *Nature* 442(7104), 797 (2006)
5. S. Mühlbauer, B. Binz, F. Jonietz, C. Pfleiderer, A. Rosch, A. Neubauer, R. Georgii, and P. Böni, Skyrmion lattice in a chiral magnet, *Science* 323(5916), 915 (2009)
6. X. Z. Yu, Y. Onose, N. Kanazawa, J. H. Park, J. H. Han, Y. Matsui, N. Nagaosa, and Y. Tokura, Real-space observation of a two-dimensional skyrmion crystal, *Nature* 465(7300), 901 (2010)
7. X. Z. Yu, N. Kanazawa, Y. Onose, K. Kimoto, W. Z. Zhang, S. Ishiwata, Y. Matsui, and Y. Tokura, Near room-temperature formation of a skyrmion crystal in thin-films of the helimagnet FeGe, *Nat. Mater.* 10(2), 106 (2011)
8. S. Heinze, K. von Bergmann, M. Menzel, J. Brede, A. Kubetzka, R. Wiesendanger, G. Bihlmayer, and S. Blügel, Spontaneous atomic-scale magnetic skyrmion lattice in two dimensions, *Nat. Phys.* 7(9), 713 (2011)
9. T. Schulz, R. Ritz, A. Bauer, M. Halder, M. Wagner, C. Franz, C. Pfleiderer, K. Everschor, M. Garst, and A. Rosch, Emergent electrodynamics of skyrmions in a chiral magnet, *Nat. Phys.* 8(4), 301 (2012)
10. A. Neubauer, C. Pfleiderer, B. Binz, A. Rosch, R. Ritz, P. G. Niklowitz, and P. Boni, Topological Hall effect in the *A* phase of MnSi, *Phys. Rev. Lett.* 102(18), 186602 (2009)

11. N. Kanazawa, Y. Onose, T. Arima, D. Okuyama, K. Ohoyama, S. Wakimoto, K. Kakurai, S. Ishiwata, and Y. Tokura, Large topological Hall effect in a short-period helimagnet MnGe, *Phys. Rev. Lett.* 106(15), 156603 (2011)
12. J. D. Zang, M. Mostovoy, J. H. Han, and N. Nagaosa, Dynamics of skyrmion crystals in metallic thin films, *Phys. Rev. Lett.* 107(13), 136804 (2011)
13. N. Romming, C. Hanneken, M. Menzel, J. E. Bickel, B. Wolter, K. von Bergmann, A. Kubetzka, and R. Wiesendanger, Writing and deleting single magnetic skyrmions, *Science* 341(6146), 636 (2013)
14. J. Sampaio, V. Cros, S. Rohart, A. Thiaville, and A. Fert, Nucleation, stability and current-induced motion of isolated magnetic skyrmions in nanostructures, *Nat. Nanotechnol.* 8(11), 839 (2013)
15. J. Iwasaki, M. Mochizuki, and N. Nagaosa, Current-induced skyrmion dynamics in constricted geometries, *Nat. Nanotechnol.* 8(10), 742 (2013)
16. Y. F. Li, N. Kanazawa, X. Z. Yu, A. Tsukazaki, M. Kawasaki, M. Ichikawa, X. F. Jin, F. Kagawa, and Y. Tokura, Robust formation of skyrmions and topological Hall effect anomaly in epitaxial thin films of MnSi, *Phys. Rev. Lett.* 110(11), 117202 (2013)
17. Y. Zhou and M. Ezawa, A reversible conversion between a skyrmion and a domain-wall pair in a junction geometry, *Nat. Commun.* 5(1), 4652 (2014)
18. W. Jiang, P. Upadhyaya, W. Zhang, G. Yu, M. B. Jungfleisch, F. Y. Fradin, J. E. Pearson, Y. Tserkovnyak, K. L. Wang, O. Heinonen, S. G. E. te Velthuis, and A. Hoffmann, Blowing magnetic skyrmion bubbles, *Science* 349(6245), 283 (2015)
19. A. O. Leonov, T. L. Monchesky, N. Romming, A. Kubetzka, A. N. Bogdanov, and R. Wiesendanger, The properties of isolated chiral skyrmions in thin magnetic films, *New J. Phys.* 18(6), 065003 (2016)
20. W. J. Jiang, X. C. Zhang, G. Q. Yu, W. Zhang, X. Wang, M. B. Jungfleisch, J. E. Pearson, X. M. Cheng, O. Heinonen, K. L. Wang, Y. Zhou, A. Hoffmann, and S. G. E. te Velthuis, Direct observation of the skyrmion Hall effect, *Nat. Phys.* 13(2), 162 (2017)
21. K. Litzius, I. Lemesh, B. Kruger, P. Bassirian, L. Caretta, K. Richter, F. Buttner, K. Sato, O. A. Tretiakov, J. Forster, R. M. Reeve, M. Weigand, L. Bykova, H. Stoll, G. Schutz, G. S. D. Beach, and M. Klaui, Skyrmion Hall effect revealed by direct time-resolved X-ray microscopy, *Nat. Phys.* 13(2), 170 (2017)
22. P. J. Hsu, A. Kubetzka, A. Finco, N. Romming, K. von Bergmann, and R. Wiesendanger, Electric-field-driven switching of individual magnetic skyrmions, *Nat. Nanotechnol.* 12(2), 123 (2016)
23. N. Nagaosa and Y. Tokura, Topological properties and dynamics of magnetic skyrmions, *Nat. Nanotechnol.* 8(12), 899 (2013)
24. R. Wiesendanger, Nanoscale magnetic skyrmions in metallic films and multilayers: A new twist for spintronics, *Nat. Rev. Mater.* 1(7), 16044 (2016)
25. A. Fert, N. Reyren, and V. Cros, Magnetic skyrmions: Advances in physics and potential applications, *Nat. Rev. Mater.* 2(7), 17031 (2017)
26. W. Kang, Y. Huang, X. C. Zhang, Y. Zhou, and W. Zhao, Skyrmion-electronics: An overview and outlook, *Proc. IEEE* 104(10), 2040 (2016)
27. S. Woo, K. M. Song, X. Zhang, M. Ezawa, Y. Zhou, X. Liu, M. Weigand, S. Finizio, J. Raabe, M. C. Park, K. Y. Lee, J. W. Choi, B. C. Min, H. C. Koo, and J. Chang, Deterministic creation and deletion of a single magnetic skyrmion observed by direct time-resolved X-ray microscopy, *Nat. Electron.* 1(5), 288 (2018)
28. I. Dzyaloshinsky, A thermodynamic theory of "weak" ferromagnetism of antiferromagnetics, *J. Phys. Chem. Solids* 4(4), 241 (1958)
29. T. Moriya, Anisotropic superexchange interaction and weak ferromagnetism, *Phys. Rev.* 120(1), 91 (1960)
30. S. A. Siegfried, E. V. Altynbaev, N. M. Chubova, V. Dyadkin, D. Chernyshov, E. V. Moskvin, D. Menzel, A. Heinemann, A. Schreyer, and S. V. Grigoriev, Controlling the Dzyaloshinskii–Moriya interaction to alter the chiral link between structure and magnetism for $Fe_{1-x}Co_xSi$, *Phys. Rev. B* 91(18), 184406 (2015)
31. T. Koretsune, N. Nagaosa, and R. Arita, Control of Dzyaloshinskii–Moriya interaction in $Mn_{1-x}Fe_xGe$: A first-principles study, *Sci. Rep.* 5(1), 13302 (2015)
32. X. Ma, G. Yu, X. Li, T. Wang, D. Wu, K. S. Olsson, Z. Chu, K. An, J. Q. Xiao, K. L. Wang, and X. Li, Interfacial control of Dzyaloshinskii–Moriya interaction in heavy metal/ferromagnetic metal thin film heterostructures, *Phys. Rev. B* 94, 180408(R) (2016)
33. A. Belabbes, G. Bihlmayer, S. Blügel, and A. Manchon, Oxygen-enabled control of Dzyaloshinskii–Moriya Interaction in ultra-thin magnetic films, *Sci. Rep.* 6(1), 24634 (2016)
34. A. L. Balk, K.-W. Kim, D. T. Pierce, M. D. Stiles, J. Unguris, and S. M. Stavis, Simultaneous control of the Dzyaloshinskii–Moriya interaction and magnetic anisotropy in nanomagnetic trilayers, *Phys. Rev. Lett.* 119, 077205 (2017)
35. G. Beutier, S. P. Collins, O. V. Dimitrova, V. E. Dmitrienko, M. I. Katsnelson, Y. O. Kvashnin, A. I. Lichtenstein, V. V. Mazurenko, A. G. A. Nisbet, E. N. Ovchinnikova, and D. Pincini, Band filling control of the Dzyaloshinskii–Moriya interaction in weakly ferromagnetic insulators, *Phys. Rev. Lett.* 119(16), 167201 (2017)
36. T. Srivastava, M. Schott, R. Juge, V. Křižaková, M. Belmeguenai, Y. Roussigné, A. Bernand-Mantel, L. Ranno, S. Pizzini, S. M. Cherif, A. Stashkevich, S. Auffret, O. Boulle, G. Gaudin, M. Chshiev, C. Baraduc, and H. Béa, Large-voltage tuning of Dzyaloshinskii–Moriya interactions: A route toward dynamic control of skyrmion chirality, *Nano Lett.* 18(8), 4871 (2018)
37. I. A. Ado, A. Qaiumzadeh, R. A. Duine, A. Brataas, and M. Titov, Asymmetric and symmetric exchange in a generalized 2D Rashba ferromagnet, *Phys. Rev. Lett.* 121(8), 086802 (2018)

38. J. Suwardy, K. Nawaoka, J. Cho, M. Goto, Y. Suzuki, and S. Miwa, Voltage-controlled magnetic anisotropy and voltage-induced Dzyaloshinskii–Moriya interaction change at the epitaxial Fe(001)/MgO(001) interface engineered by Co and Pd atomic-layer insertion, *Phys. Rev. B* 98(14), 144432 (2018)

39. A. Cao, X. Zhang, B. Koopmans, S. Peng, Y. Zhang, Z. Wang, S. Yan, H. Yang, and W. Zhao, Tuning the Dzyaloshinskii–Moriya interaction in Pt/Co/MgO heterostructures through the MgO thickness, *Nanoscale* 10(25), 12062 (2018)

40. H. Yang, O. Boulle, V. Cros, A. Fert, and M. Chshiev, Controlling Dzyaloshinskii–Moriya interaction via chirality dependent atomic-layer stacking, insulator capping and electric field, *Sci. Rep.* 8(1), 12356 (2018)

41. S. A. Díaz and R. E. Troncoso, Controlling skyrmion helicity via engineered Dzyaloshinskii–Moriya interactions, *J. Phys.: Condens. Matter* 28, 426005 (2016)

42. R. Menezes, J. Mulkers, C. C. de Souza Silva, and M. V. Miloević, Deflection of ferromagnetic and antiferromagnetic skyrmions at heterochiral interfaces, *Phys. Rev. B* 99, 104409 (2019)

43. A. O. Leonov and I. Kézsmárki, Skyrmion robustness in noncentrosymmetric magnets with axial symmetry: The role of anisotropy and tilted magnetic fields, *Phys. Rev. B* 96(21), 214413 (2017)

44. S. Seki and M. Mochizuki, Skyrmions in Magnetic Materials, Springer, Switzerland, 2016

45. X. S. Wang, H. Y. Yuan, and X. R. Wang, A theory on skyrmion size, *Commun. Phys.* 1(1), 31 (2018)